Aalto University

Daskalakis, Konstantinos S.; Freire-Fernández, Francisco; Moilanen, Antti J.; Van Dijken, Sebastiaan; Törmä, Päivi

Converting an organic light-emitting diode from blue to white with bragg modes

Converting an Organic Light-Emitting Diode from Blue to White with Bragg Modes

Konstantinos S. Daskalakis,* Francisco Freire-Fernández, Antti J. Moilanen, Sebastiaan van Dijken, and Päivi Törmä*

COMP Centre of Excellence, Department of Applied Physics, Aalto University School of Science, FI-00076 Aalto, Finland

S *Supporting Information*

ABSTRACT: Organic light-emitting diodes (OLEDs) have been established as versatile light sources that allow for easy integration in large-area surfaces and flexible substrates. In addition, the low fabrication cost of OLEDs renders them particularly attractive as general lighting sources. Current methods for the fabrication of white-light OLEDs rely on the combination of multiple organic emitters and/or the incorporation of multiple cavity modes in a thick active medium. These architectures introduce formidable challenges in both device design and performance improvements, namely, the decrease of efficiency with increasing brightness (efficiency roll-off) and short operational lifetime. Here we demonstrate, for the first time, white-light generation in an OLED consisting of a sub-100 nm thick blue single-emissive layer coupled to the photonic Bragg modes of a dielectric distributed Bragg reflector (DBR). We show that the Bragg modes, although primarily located inside the DBR stack, can significantly overlap with the emissive layer, thus efficiently enhancing emission and outcoupling of photons at selected wavelengths across the entire visible light spectrum. Moreover, we show that color temperature can be tuned by the DBR parameters, offering great versatility in the optimization of white-light emission spectra.

KEYWORDS: *organic semiconductors, distributed Bragg reflector, white organic light-emitting diodes (WOLEDs), Fabry−Pérot modes, electroluminescence color conversion*
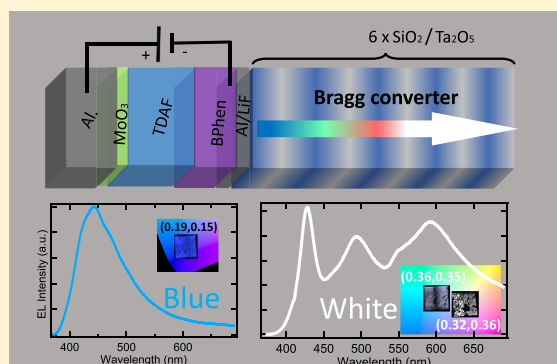
T hree decades ago, a twist in the search of an efficient illumination source came from the demonstration of a practical organic light-emitting diode (OLED).[1] Since then, OLEDs have been utilized in a plethora of optoelectronic applications,[2,3] and the effort for improving their efficiency constitutes one of the major trends in modern optoelectronics research.[4−6] Owing to their low fabrication cost, exceptional color rendering, and ease of deposition to large areas and flexible substrates, OLEDs have attracted a lot of attention as general illumination devices in which broadband and high-intensity white light is a key requirement.[7,8] Although single-emitter OLEDs have spectral bandwidth which predominantly covers only a part of the visible spectrum, numerous demonstrations of white-emitting OLEDs (WOLEDs) have been reported.[9−11]

Generally, reported methods for the realization of WOLEDs by materials design can be categorized as follows: (1) WOLEDs consisting of multiple vertically stacked emissive layers or horizontally striped structures. White light in these architectures is created by a mixture of independently emitting red, green, and blue OLEDs. While these strategies offer stable electro-luminescence and high device yields, the active area is thick, which usually results in high operating current. Achieving the desired color balance requires precise control over the thickness and composition of each layer which makes the fabrication of such WOLEDs complicated, rendering them incompatible as

inexpensive solid-state lighting sources.[11,12] (2) Single-emissive layer structures in which white light is achieved via near-molecule energy transfer (Förster or Dexter) between a matrix material and multiple dopant emitters. These structures are easy to fabricate either by vacuum deposition or solution processes. Major disadvantages of this method are precise control of the dopant concentration and the operational voltages required for reliable control of the electroluminescence spectrum.[11,12] (3) Single-emissive layer with bimolecular excited species, such as excimers and exciplexes.[13,14] While these species harvest the otherwise undesired losses in red-shifted emission bands to generate white light, color tunability and high-power stability remain challenges.

In addition to the aforementioned material optimization and device engineering methods, white-light emission in OLEDs has been reported by introducing a photonic design such as microcavities with multiple resonances. There, cavity modes are confined in a thick active region between highly reflective metallic mirrors, or a combination of metallic and distributed Bragg reflector (DBR) mirrors. The emissive layer has a broadband visible emission spectrum which is either Purcell-enhanced or suppressed by the cavity modes.[15,16] Because the
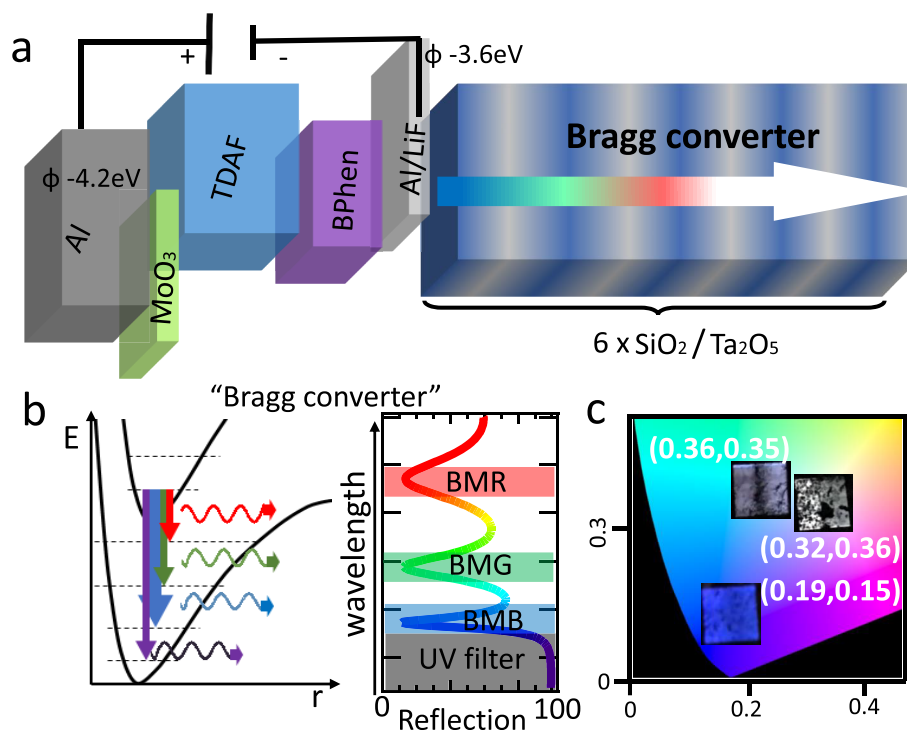
Figure 1. (a) Schematic of the Bragg WOLED concept. Electroluminescence from a 50 nm TDAF emissive layer occurs through the Bragg modes of a dielectric DBR mirror (6-pair SiO_2/Ta_2O_5). The asymmetric alignment of the layers represents the work functions of the materials. (b) Schematic illustration of the white-light generation mechanism, which we call Bragg conversion, in our devices. On the left, a simplified diagram of electronic states and transitions that produce photons in molecular semiconductors is shown. The arrows pointing down represent the radiative transitions, and their thicknesses illustrate the transition rates (thicker arrow means larger rate leading to more photons). On the right, the reflectivity of a Bragg converter is depicted. Its high-reflectivity photonic stopband acts as a long pass filter, blocking ultraviolet radiation (grayed-out area), while the transparency Bragg modes, located out of the photonic stopband, are resonant with the molecular transitions that radiate visible photons (Bragg mode blue, green, and red; or BMB, BMG, and BMR, respectively). (c) CIE map, together with the corresponding CIE coordinates. Device dimensions are 3 $\times$ 3 mm^2.

color ratio of red, green, and blue is primarily defined by the optical modes, the white-light spectrum is expected to be uninfluenced by variations in doping, carrier competition, and other molecular emission instabilities. Such photonic multi-resonant structures are advantageous because they can be designed to utilize emissive layer(s) from any of the previously discussed categories. However, there are two main challenges in such multimode WOLEDs: (a) While metal-clad microcavities have a broad reflectivity band, and they can support multiple modes, they suffer from emission losses as light has to exit a thick metallic layer. (b) The increased cavity length (usually thicker than $3\lambda/2$, where λ is the wavelength of light) introduces additional lossy waveguide. There, several modeling techniques can be employed to describe the increase of emission efficiencies.[17,18] Also, thick cavities result in an increased electron–hole propagation distance which impedes efficient electron–hole recombination in OLEDs and can also lead to efficiency roll-off due to increased bimolecular annihilation processes,[19] with the exception of the recent breakthrough by Matsushima et al.[20] Another approach for producing white electroluminescence is the hybridization of a single cavity mode with a Tamm plasmon–polariton resonance.[21] These hybrid modes can strongly outcouple electroluminescence at two different colors, resulting in white light. While this light outcoupling strategy allows for independent optimization between electrical and optical efficiency, the mode hybridization makes the device design complicated.[22]

Here, we present a proof-of-concept experimental demonstration of a device architecture to convert monochromatic blue fluorescent OLEDs to WOLEDs efficiently. We observed broadband white-light emission from a blue OLED by utilizing Bragg modes, which are Fabry–Pérot modes in the DBR slab, with resonances at red, green, and blue colors. We demonstrate that although the Bragg modes primarily reside inside the DBR stack, they can significantly overlap with the emissive layer, thus enhancing emission and outcoupling of photons at selected wavelengths over the entire visible spectrum. In our device architecture, the dielectric DBR is directly deposited on a top-emitting, single-emissive layer OLED. Instead of usage as a cavity, the photonic stopband of the DBR is designed to block unwanted ultraviolet electroluminescence. We call this novel device design a "Bragg converter". The DBR stopband and the Bragg modes can be independently designed as the former depends on the period of the stack and the latter on its total thickness. Importantly, the Bragg modes which are determined by the DBR stack thickness are broad and do not require high-quality DBRs with precisely controlled layer thicknesses. To our knowledge, this is the only WOLED device design wherein the internal quantum efficiency can be optimized independently of the color temperature.

■ WOLED DEVICE

A schematic of our WOLED is shown in Figure 1a. It consists of a 50 nm layer of 2,7-bis [9,9-di(4-methylphenyl)-fluoren-2-yl]-9,9-di(4-methylphenyl) fluorene (TDAF) sandwiched between
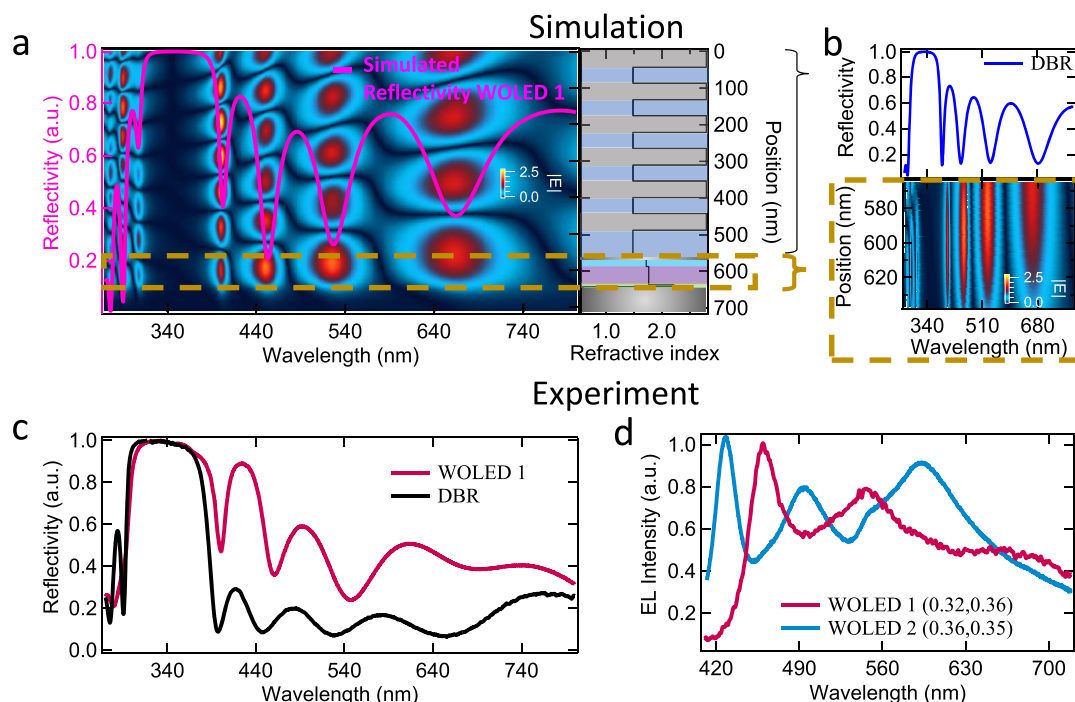
Simulation

Experiment

Figure 2. (a) Transfer-matrix simulation of reflectivity (pink axis on the left) and electric field intensity (background contour map) as a function of the wavelength and position inside the WOLED 1 structure. Reflectivity and electric field were calculated at normal incidence angle. On the right is shown a schematic of the simulated structure WOLED 1; the colors denote different materials as defined in Figure 1a. The right axis, position (nm), refers to the thickness of the layers in the device where the 0 nm position refers to the top-side of the WOLED device. The black lines show the refractive index change for a propagating plane wave with $\lambda = 441$ nm. (b) Simulated reflectivity of the Bragg converter, top-570 nm thick layers, and electric field intensity map in the electroluminescent region of the WOLED (from 563 to 637 nm), highlighted with a brown dashed-line rectangular box. (c) Reflectivity measurements of the Bragg converter on glass (black) and as a WOLED (passive structure, no current injection) (red). Note the perfect match of simulated (a, pink line) and measured (c) modes. (d) Normal incidence top-side electroluminescence (EL) from the designed device WOLED 1 (red) and a second WOLED device with different DBR layer content (53 nm SiO_2/42 nm Ta_2O_5), denoted WOLED 2 (blue).

a 70 nm Al bottom anode with a 5 nm MoO_3 hole-injecting layer and a 10 nm LiF/Al cathode with a 20 nm 4,7-diphenyl-1,10-phenanthroline (BPhen) hole-blocking layer. The DBR consisting of 6 alternating layers of SiO_2 and Ta_2O_5 was directly sputtered on top of the Al cathode, thus providing encapsulation of the organic materials (Figure S2). TDAF was chosen as the single-emissive layer material due to its pure-hydrocarbon structure (family of oligofluorenes) which contains the sp^3-hybridized C-9 of fluorene. This gives TDAF high thermal and morphological stability so that it can withstand aggressive processing steps such us the sputtering of the dielectric DBR top-mirror. Moreover, TDAF has ambipolar nature, rendering it capable of electroluminescence.[23] In the past few years, TDAF has enabled the observation of nonequilibrium polariton condensation at room temperature.[24−26]

Figure 1b illustrates our concept for converting a blue-emitting OLED to a WOLED. After electrical injection of electron and hole carriers, the exciton formation and relaxation results in radiation of photons with different rates as illustrated by downward pointing arrows in the left panel of Figure 1b. The incorporation of cavity modes or other near-field modes that are resonant with the molecular transitions results in an increase of the radiation rate at the resonant frequencies and suppression of other radiation paths. The effect of the Bragg converter is demonstrated in Figure 1c where the Commission Internatio-nale de l'Eclairage (CIE) map shows the coordinates and pictures of our OLED devices before the DBR encapsulation [blue OLED, CIE (0.19, 0.15)] and after. Different thicknesses of the SiO_2 and Ta_2O_5 alternating layers result in shifting of the

Bragg modes and tuning of the color temperature. As an example, a 6-pair DBR with 43 nm SiO_2 and 41 nm Ta_2O_5 (WOLED 1) thickness produced white electroluminescence with temperature 6007 K (daylight), and 53 nm SiO_2 and 42 nm Ta_2O_5 (WOLED 2) thickness produced white light with temperature 4450 K (cool white).

■ BRAGG CONVERTER

DBR is a superlattice structure consisting of two alternating layers of low and high refractive index materials and is generally used as a high-reflectivity nonabsorbing narrow-band mirror. The desired band of reflection, called stopband, is a result of constructive interference of light reflected from the layer boundaries. Outside the photonic stopband spectral range, one can identify a succession of high-transparency modes, called Bragg modes, that appear with a period of $2L_{DBR}n_{eff}/\lambda_{vac}$, where L_{DBR} is the thickness, n_{eff} is the effective refractive index of the superlattice, and λ_{vac} is the vacuum wavelength of the light. Unlike cavity modes, the Bragg mode field antinodes do not concentrate in the central region of an optical cavity, namely, the spacer layer in between two highly reflective mirrors. Instead, Bragg modes are localized mostly inside and at the surfaces of the superlattice slab. This is clearly shown in Figure 2a,b where we used a typical transfer-matrix method[27] to calculate the electric field antinodes of a DBR sandwiching the blue top-emitting OLED.

By using the measured material parameters (see the Methods section), we can design a DBR such that its stopband acts as an ultraviolet radiation inhibitor while emission of photons occurs
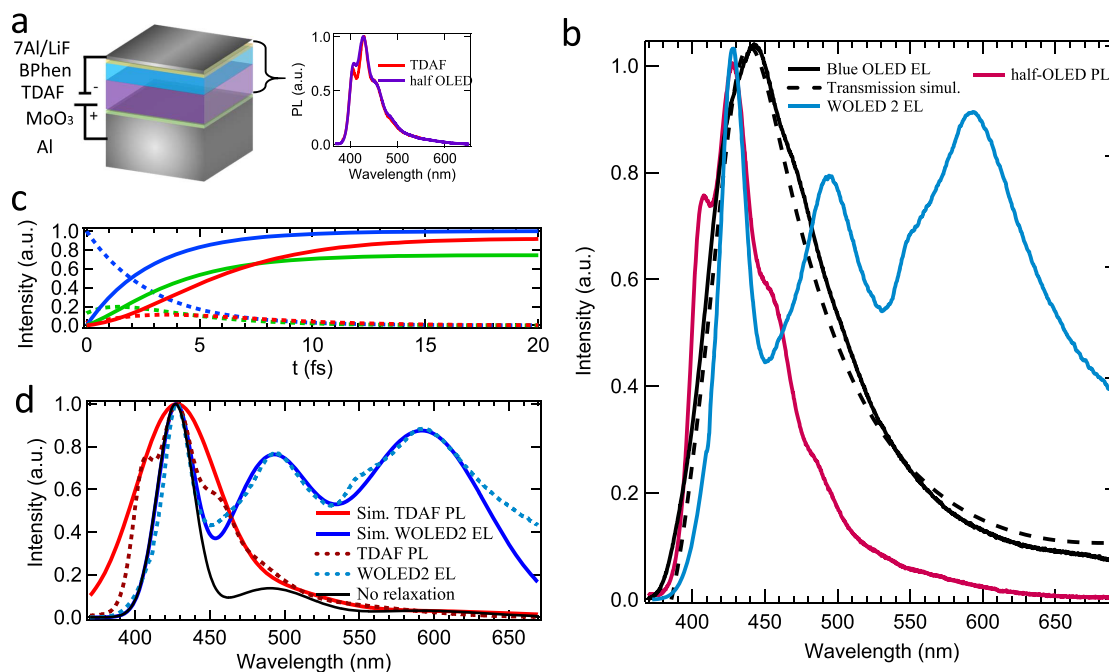
Figure 3. (a) Left: schematic of the OLED before its encapsulation with the DBR. Right: the photoluminescence (PL) spectra are identical for bare TDAF film and a half OLED structure (a multilayer of TDAF, BPhen, LiF, and 7 nm Al). (b) Comparison between normalized photoluminescence from a half OLED (red line, half-OLED PL) and a blue OLED before (black, blue OLED EL) and after its integration to the Bragg converter and conversion to WOLED 2 (WOLED 2 EL). The electroluminescence was obtained at 35 mA/cm^2. The dashed line shows the calculated transmission (electroluminescence) for the blue OLED. (c) Rate-equation simulation. The dashed lines present the input weights of blue, green, and red colors. The initial weights at time 0 s are obtained from the photoluminescence spectrum of the bare TDAF film by fitting three Gaussian profiles at wavelengths 427, 490, and 592 nm (red solid line in part d). The normalized output color weights are shown by the solid lines. (d) Rate-equation simulation results after the steady-state has been reached. The steady-state intensities are illustrated with three Gaussians centered at wavelengths 427, 490, and 592 nm (blue solid line). The black line represents the simulated spectrum without relaxation processes included. The dashed lines present the measured TDAF photoluminescence (red) and WOLED 2 electroluminescence (blue) for comparison.

through the Bragg modes. At visible wavelengths, the effective thickness (dispersive refractive index of SiO$_2$ and Ta$_2$O$_5$) of our Bragg converter exhibits Bragg modes that perfectly match the blue, green, and red wavelengths (450, 540, and 640 nm), while their broad line width is essential for broadband white-light generation. Moreover, the Bragg mode spectrum changes negligibly when we incorporate the thin OLED in the Bragg converter design. This can be seen in the simulation in Figure 2a,b and the reflectivity experiment in Figure 2c. In Figure 2a,b, electric field was calculated with a resolution of 1 nm. The thin emitter layer between the metal and the DBR does not have any cavity modes within the DBR stopband (where reflectivity is 1.0); we focus solely on the use of the Bragg modes that are spectrally outside the stopband. Note that the Bragg modes have regions of high field intensity overlapping with the emitter layer, Figure 2a. Therefore, by simply controlling the DBR effective thickness, Bragg modes can be designed to have desired wavelengths and to significantly overlap with the emitter layer so that electroluminescence is efficiently coupled into these modes.

The astounding conversion performance of the Bragg modes is shown in Figure 2d presenting the generation of white electroluminescence from a blue OLED. Here, we see that the WOLED 1 produced daylight white (6007 K) electroluminescence with main peaks at three of the Bragg modes predicted by the transfer-matrix simulation and measured in reflectivity. We also demonstrate the tunability of our Bragg converter by another device (WOLED 2) with different DBR layer content, producing cool white (4450 K) electroluminescence. In the past years, many works have focused on

demonstrating white electroluminescence through high-quality multiresonant cavity modes. While high-quality cavity modes are the key elements for amplification and lasing and can provide narrow emission,[15,16] they also suppress emission from non-resonant states, which reduces the external quantum efficiency and increases internal thermal losses and efficiency roll-off. Another advantage of our Bragg converter is that the Bragg modes are insensitive to DBR layer imperfections, such as thickness variations and interface roughness. Moreover, the Bragg modes can be tuned independently of the stopband by changing the total thickness of the DBR, thus allowing for simultaneous optimization of stopband and Bragg mode designs.

To comprehend the electroluminescence mechanism in our WOLEDs, we studied the emission properties of the top-emitting blue OLEDs (part of our WOLEDs) without the DBR. A schematic and measured photoluminescence of the OLED are shown in Figure 3a. Electroluminescence from our OLEDs occurs from the top-side and is inhomogeneous and spectrally broad (full-width at half-maximum from 420 to 520 nm) with a central peak at 450 nm, Figure 3b. We used a ∼7 nm thick top Al cathode to avoid absorption losses when the OLED is integrated to the Bragg converter. At 7 nm thickness the Al films showed more than 50% transparency while still being conductive. Similar OLEDs with thicker top cathode (32 nm) have shown ultrastrong coupling[24] and electroluminescence from the lower polariton branch.[28] The shape of the emission is strongly influenced by the interface of the top Al/LiF and air that creates a cavity effect (half-wavelength in the 100 nm size of the emitter layer, with refractive index around two, corresponds to roughly
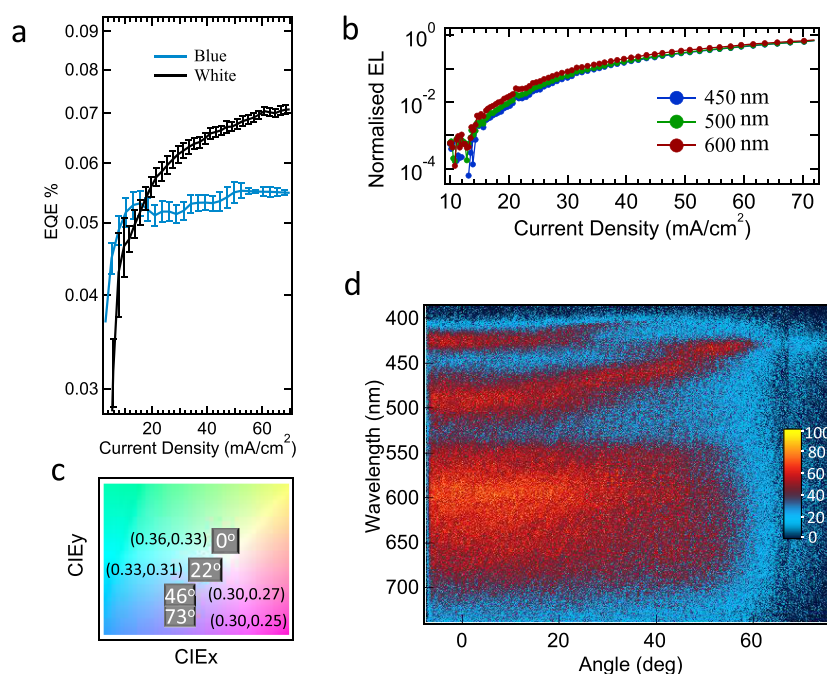
Figure 4. (a) External quantum efficiency (EQE) comparison between the OLEDs before and after encapsulation in the Bragg converter. Error bars here are standard deviations from the average value of three different devices measured three times each. (b) Current-dependent electroluminescence (EL) intensity at the three main spectral locations 450, 500, and 600 nm of the WOLED 2 device. (c) CIE map of WOLED 2 electroluminescence at incidence angles of 0°, 22°, 46°, and 73°, with a detection half angle of 5°. The CIE coordinates from top to bottom correspond to color temperatures 4450, 6214, 8669, and 9886 K. (d) Angle-resolved electroluminescence map of WOLED 2. This map was used to determine the CIE values in part c.

400 nm emitted light), as is confirmed by the transfer-matrix simulation of the transmission. By performing a current-dependent electroluminescence measurement of the OLED, we observed that the shape of the spectra remained unchanged upon increasing current and power (Figure S3). Therefore, for the studied range of injection currents (power), the electro-luminescence mechanism was not influenced by emission from power-induced excitonic species.

Comparing the OLED emission before and after conversion to WOLED 2, we see that (Figure 3b) the Bragg converter vastly modified the emission. The most striking effect is the 10-fold increase of electroluminescence at the red color (630 nm). This further highlights that the existence of Bragg modes and their strong field intensity overlapping with the emitter layer greatly improves the outcoupling. To confirm that the red-shifted emission resulted from efficient Bragg outcoupling and not from sample contamination, we used a 200 fs pulsed laser at 360 nm to optically excite the top-half of the blue OLED. As shown in the right panel of Figure 3a, photoluminescence of a pristine TDAF film and a multilayer of TDAF, BPhen, LiF, and 7 nm Al is identical, verifying that radiation in our devices occurred from a single-emissive layer, the TDAF.

We have devised a heuristic rate-equation model to describe the observed electroluminescence spectrum of the WOLED. The model assumes three bands at different energies, corresponding to the Bragg modes at red, green, and blue wavelengths. The bands have different lifetimes (outcoupling rates) and relaxation rates from higher-energy bands toward lower-energy bands. We used lifetimes based on the quality factors of the simulated Bragg modes. Initial weights of population in the modes were taken from the bare TDAF photoluminescence. See the Supporting Information for details of the model. The relaxation rates were essentially fitting parameters, determined by a comparison to the experiment.

Assuming that the relaxation is slightly more efficient toward lower energies, we can reproduce the measured WOLED electroluminescence spectrum, see Figure 3d. The time evolutions of the input (dashed lines) and the output (solid lines) bands are presented in Figure 3c. The steady-state values show that the initial weighting of colors has changed drastically, such that in the end red and green wavelengths are highly intensified with respect to blue. For comparison, we present in Figure 3d also the spectrum for the case without any relaxation. Thus, the model suggests that relaxation effects are essential, in addition to the efficient outcoupling by the Bragg modes. Such relaxation mechanisms are known to take place under high electrical excitation; for instance, the electric field modifies the potential landscape between molecular species creating intermolecular excited states (electroplexes) and low-lying triplet states.[29] Understanding the role of relaxation mechanisms in our results is an important topic of future research since it provides one more way to improve the device performance.

CONVERSION PERFORMANCE AND CHROMATICITY

Remarkably, by comparing the external quantum efficiency of the blue OLED and Bragg-converted WOLEDs as a function of injection current, we observed a 20% increase above 40 mA/cm^2. Our photonic structures can also be combined with emitters with high internal quantum efficiency, as long as the spectrum of the emitter is similar to TDAF. As shown in Figure 4a, the low external quantum efficiency of the blue OLED reaches a plateau value at ∼10 mA/cm^2 while the external quantum efficiency of the WOLED continues to increase. This shows that the relaxation processes to red-shifted wavelengths and outcoupling by the Bragg modes improve the overall efficiency of the WOLED. The increase of external quantum efficiency partially comes from relaxation to the less absorbing

spectral region of the WOLED (Figure S5), but it could be also attributed to the efficient outcoupling of emission from bimolecular excited states formed in the interface of TDAF and BPhen.[30,31] Note that the Bragg converter concept can also be potentially utilized in other contexts, such as for harvesting energy from long-lived triplet states either through strong coupling[32−34] (Figure S4) or by typical photon upconversion or phosphorescence mechanisms.[35,36] In addition to the improved external quantum efficiency, the encapsulation of the OLED in the dielectric Bragg converter results in a more than 30-fold increase of on-shelf lifetime compared to nonencapsulated OLED (Figure S2). Figure 4b shows the WOLED 2 current-dependent electroluminescence intensity at three main spectral locations 450, 500, and 600 nm. The chromaticity of the WOLEDs remained stable for the measured range of applied powers. Even when our WOLEDs are multilayer structures, the color temperature remained stable for detection angles up to ~25° (Figure 4c). For detection angles >25°, electroluminescence from our WOLEDs becomes increasingly blue, and the color temperature might not apply. Figure 4d shows the measured angle-dependent chromaticity of the WOLED 2 device by collecting momentum-resolved images from −7° to 78°. A transfer-matrix simulation of the angle-dependent reflectivity of the WOLED 2 is shown in the Supporting Information, Figure S8.

■ CONCLUSIONS

We have experimentally demonstrated the conversion of a single-emissive layer OLED from blue to white by utilizing the Bragg modes of a dielectric distributed Bragg reflector (DBR). In our novel concept of single-emitter WOLEDs, the reflectivity stopband of the DBR was used for suppressing emission in the ultraviolet, while electroluminescence outcoupling was tailored by utilizing the Bragg modes. The experimental findings were supported by theoretical analysis. Transfer-matrix simulations showed that the Bragg modes can be localized in the emissive layer and reach high field intensities, which is in agreement with the efficient outcoupling. A rate-equation model reproduced the Bragg-conversion concept and indicated that relaxation processes play a role in the white-light generation. Color temperature tuning in our WOLEDs was achieved by changing the thicknesses of the alternating superlattice layers and thereby the size of the DBR. Moreover, the WOLED devices showed a 20% increase of external quantum efficiency and 30-fold increase of on-shelf lifetime, as compared with the nonconverted blue OLED. Our device architecture does not depend on the substrate and incorporates metallic contacts instead of indium tin oxide films which are difficult to control and contain the scarce material indium. The Bragg modes do not require precise layer thicknesses which means low-quality, low-cost DBRs such as all-plastic ones can be used.[37,38] Importantly, the color temperature depends on the DBR while the internal quantum efficiency depends on the preconversion OLED. Naturally, changing the emitter to something other than TDAF can also affect the color temperature. The internal quantum efficiency and color temperature can therefore be optimized independently; thus, our Bragg conversion mechanism offers prospects for utilizing highly efficient and stable blue thermally activated delay fluorescent (TADF) materials.[39,40] Also, the use of a sub-100 nm thick single-emissive layer can enable the suppression of losses from waveguided modes while allowing for efficient recombination of electrons and holes. Our result essentially shows that efficient and high-quality broadband white-light generation does not require high-quality cavity modes. Therefore, we believe, our Bragg converter concept is the most promising method for suppressing the efficiency roll-off in WOLEDs. Moreover, the ability to create multiple modes with high field intensities in the emissive layer offers prospects for strong coupling studies, with potential applications in harvesting precious triplet energy from existing low-cost and stable organic emitters.

■ METHODS

Device Fabrication. The OLED part of the devices was fabricated by standard vacuum evaporation methods (Edwards E306). All the films were deposited at a base pressure of ~10^{-6} mbar and deposition rate of 2 Å/s. We used square 15 × 15 mm quartz substrates on which we patterned 4 square OLEDs with dimensions 3 × 3 mm. To avoid deposition shadowing effects, 500 μm thick aluminum shadow masks were directly in contact with the substrates. Fabrication of the OLEDs was performed in two stages that involved venting to atmospheric conditions and mask exchange. We first deposited the bottom Al anode and MoO_3 hole injection layer using e-beam deposition. For the deposition of the second half of the OLED we utilized resistive thermal sources for the organic TDAF and BPhen layers and e-beam sources for the LiF and Al layers. To encapsulate the OLEDs with the Bragg converter, we vented in atmospheric conditions and transferred the devices to a sputtering deposition system (Kurt J. Lesker). A 6-pair superlattice of SiO_2 and Ta_2O_5 was directly sputtered on top of the OLED. SiO_2 films were produced by RF sputtering from a SiO_2 target while Ta_2O_5 films were reactively sputtered from a Ta target using a 20:10 sccm $Ar:O_2$ gas-flow ratio. A combination of ellipsometry (J.A. Woollam M2000) and profilometry (Bruker DektakXT) was used to obtain the film thicknesses and optical constants.

Characterization. Schematics of the optical and electrical setups are shown in Figure S1. We used a power source meter (Keithley 2602B) for the electrical characterization of the devices and an absolute calibrated 2D CCD camera (Pixis 400) coupled to a spectrometer (Acton SpectrPro 2500) to measure the forward emission (electroluminescence and photoluminescence) from the devices. Current-dependent electroluminescence was obtained by focusing the image of the device on the spectrometer slit with a detection half angle $\theta = 15°$ and magnification $M = 2.5$. Angle-resolved electroluminescence and photoluminescence were collected by rotating the sample with a goniometer at the optical axis of an objective (10×, 0.3 numerical aperture, NA), and back focal plane images were focused to the 200 μm entrance slit of the spectrometer. A vacuum microchamber that allows the rotation of the devices was developed in house. All measurements were performed at a base pressure of ~10^{-1} mbar. By using the measured spectrally integrated electroluminescence distribution for varying the collection angle, we calculated the total photon number emitted from the top surface of the devices. The external quantum efficiency is then simply the ratio between externally radiated photons and injected electrons. Normal incidence reflectivity was performed with a reflection probe fiber (200 μm cores, 6 light-fibers, 1 read fiber) coupled to a calibrated miniature spectrometer (OceanOptics USB2000). All the setups were automatized by using the previously developed data-acquisition code in LabVIEW.[41]

ASSOCIATED CONTENT

Ⓢ Supporting Information

The Supporting Information is available free of charge on the ACS Publications website at DOI: 10.1021/acsphotonics.9b01206.

Additional figures of experimental setup, $J-V-L$ characterization of the devices, current-dependent electroluminescence of blue OLEDs, transfer-matrix simulation of a blue OLED with a 32 nm thick Al top contact, absorbance of TDAF and BPhen organic films, angular dispersion electroluminescence of all-metal TDAF OLEDs, and methods for the rate equation (PDF)

AUTHOR INFORMATION

Corresponding Authors

*E-mail: konstantinos.daskalakis@aalto.fi.
*E-mail: paivi.torma@aalto.fi.

ORCID Ⓞ

Konstantinos S. Daskalakis: 0000-0002-3996-5219
Antti J. Moilanen: 0000-0002-9888-8524
Sebastiaan van Dijken: 0000-0001-6372-2252
Päivi Törmä: 0000-0003-0979-9894

Author Contributions

K.S.D. conceived the project, performed the transfer-matrix simulations, and conducted the measurements. K.S.D. and F.F.-F. fabricated the samples. A.J.M. performed the rate-equation simulations. K.S.D., A.J.M., and P.T. wrote the manuscript together with all authors. All authors discussed the results.

Notes

The authors declare the following competing financial interest(s): K.S.D. and P.T. are the inventors of a patent currently pending with Aalto University (no. 20195269, filed 3 April 2019). All the other authors declare that they have no competing interests.

REFERENCES

(1) Tang, C. W.; VanSlyke, S. A. Organic electroluminescent diodes. *Appl. Phys. Lett.* **1987**, *51*, 913−915.

(2) Kido, J.; Kimura, M.; Nagai, K. Multilayer White Light-Emitting Organic Electroluminescent Device. *Science (Washington, DC, U. S.)* **1995**, *267*, 1332−1334.

(3) Sekitani, T.; Nakajima, H.; Maeda, H.; Fukushima, T.; Aida, T.; Hata, K.; Someya, T. Stretchable active-matrix organic light-emitting diode display using printable elastic conductors. *Nat. Mater.* **2009**, *8*, 494.

(4) Baldo, M. A.; O'Brien, D. F.; You, Y. E. A. Highly efficient phosphorescent emission from organic electroluminescent devices. *Nature* **1998**, *395*, 151−154.

(5) Uoyama, H.; Goushi, K.; Shizu, K.; Nomura, H.; Adachi, C. Highly efficient organic light-emitting diodes from delayed fluorescence. *Nature* **2012**, *492*, 234.

(6) Gómez-Bombarelli, R. Design of efficient molecular organic light-emitting diodes by a high-throughput virtual screening and experimental approach. *Nat. Mater.* **2016**, *15*, 1120.

(7) Sun, Y.; Giebink, N. C.; Kanno, H.; Ma, B.; Thompson, M. E.; Forrest, S. R. Management of singlet and triplet excitons for efficient white organic light-emitting devices. *Nature* **2006**, *440*, 908−912.

(8) Reineke, S.; Lindner, F.; Schwartz, G.; Seidler, N.; Walzer, K.; Lüssem, B.; Leo, K. White organic light-emitting diodes with fluorescent tube efficiency. *Nature* **2009**, *459*, 234.

(9) D'Andrade, B. W.; Forrest, S. R. White Organic Light-Emitting Devices for Solid-State Lighting. *Adv. Mater.* **2004**, *16*, 1585−1595.

(10) Chen, S.; Deng, L.; Xie, J.; Peng, L.; Xie, L.; Fan, Q.; Huang, W. Recent Developments in Top-Emitting Organic Light-Emitting Diodes. *Adv. Mater.* **2010**, *22*, 5227−5239.

(11) Wu, Z.; Ma, D. Recent advances in white organic light-emitting diodes. *Mater. Sci. Eng., R* **2016**, *107*, 1−42.

(12) Gather, M. C.; Köhnen, A.; Meerholz, K. White Organic Light-Emitting Diodes. *Adv. Mater.* **2011**, *23*, 233−248.

(13) Xiao, P.; Huang, J.; Yu, Y.; Yuan, J.; Luo, D.; Liu, B.; Liang, D. Recent Advances of Exciplex-Based White Organic Light-Emitting Diodes. *Appl. Sci.* **2018**, *8*, 1449.

(14) Vollbrecht, J. Excimers in organic electronics. *New J. Chem.* **2018**, *42*, 11249−11254.

(15) Zhang, H.; You, H.; Wang, W.; Shi, J.; Guo, S.; Liu, M.; Ma, D. Organic white-light-emitting devices based on a multimode resonant microcavity. *Semicond. Sci. Technol.* **2006**, *21*, 1094−1097.

(16) Zhang, J.; Song, J.; Zhang, H.; Ding, H.; Guo, K.; Wei, B.; Zheng, Y.; Zhang, Z. Sunlight-like white organic light-emitting diodes with inorganic/organic nanolaminate distributed Bragg reflector (DBR) anode microcavity by using atomic layer deposition. *Org. Electron.* **2016**, *33*, 88−94.

(17) Smith, L. H.; Wasey, J. A. E.; Samuel, I. D. W.; Barnes, W. L. Light Out-Coupling Efficiencies of Organic Light-Emitting Diode Structures and the Effect of Photoluminescence Quantum Yield. *Adv. Funct. Mater.* **2005**, *15*, 1839−1844.

(18) Kim, S.-Y.; Kim, J.-J. Outcoupling efficiency of organic light emitting diodes and the effect of ITO thickness. *Org. Electron.* **2010**, *11*, 1010−1015.

(19) Murawski, C.; Leo, K.; Gather, M. C. Efficiency roll-off in organic light-emitting diodes. *Adv. Mater.* **2013**, *25*, 6801−6827.

(20) Matsushima, T.; Bencheikh, F.; Komino, T.; Leyden, M. R.; Sandanayaka, A. S. D.; Qin, C.; Adachi, C. High performance from extraordinarily thick organic light-emitting diodes. *Nature* **2019**, *572*, 502−506.

(21) Zhang, X.-L.; Feng, J.; Han, X.-C.; Liu, Y.-F.; Chen, Q.-D.; Song, J.-F.; Sun, H.-B. Hybrid Tamm plasmon-polariton/microcavity modes for white top-emitting organic light-emitting devices. *Optica* **2015**, *2*, 579.

(22) The fine line between performance improvement and device practicality. *Nat. Commun.* **2018**, *9*, 5268.

(23) Tao, Y.; Yang, C.; Qin, J. Organic host materials for phosphorescent organic light-emitting diodes. *Chem. Soc. Rev.* **2011**, *40*, 2943−2970.

(24) Kéna-Cohen, S.; Maier, S. A.; Bradley, D. D. C. Ultrastrongly Coupled Exciton-Polaritons in Metal-Clad Organic Semiconductor Microcavities. *Adv. Opt. Mater.* **2013**, *1*, 827−833.

(25) Daskalakis, K. S.; Maier, S. A.; Murray, R.; Kéna-Cohen, S. Nonlinear interactions in an organic polariton condensate. *Nat. Mater.* **2014**, *13*, 271−278.

(26) Lerario, G.; Fieramosca, A.; Barachati, F.; Ballarini, D.; Daskalakis, K. S.; Dominici, L.; De Giorgi, M.; Maier, S. A.; Gigli, G.;

Kéna-Cohen, S.; Sanvitto, D. Room-temperature superfluidity in a polariton condensate. *Nat. Phys.* **2017**, *13*, 837−841.

(27) Benisty, H.; Stanley, R.; Mayer, M. Method of source terms for dipole emission modification in modes of arbitrary planar structures. *J. Opt. Soc. Am. A* **1998**, *15*, 1192.

(28) Gubbin, C. R.; Maier, S. a.; Kéna-Cohen, S. Low-voltage polariton electroluminescence from an ultrastrongly coupled organic light-emitting diode. *Appl. Phys. Lett.* **2014**, *104*, 233302.

(29) Kalinowski, J. *Organic Light-Emitting Diodes: Principles, Characteristics, and Processes*; CRC Press, 2004.

(30) Tong, Q.-X.; Lai, S.-L.; Chan, M.-Y.; Tang, J.-X.; Kwong, H.-L.; Lee, C.-S.; Lee, S.-T. High-efficiency nondoped white organic light-emitting devices. *Appl. Phys. Lett.* **2007**, *91*, 023503.

(31) Song, L.; Hu, Y.; Liu, Z.; Lv, Y.; Guo, X.; Liu, X. Harvesting triplet excitons with exciplex thermally activated delayed fluorescence emitters toward high performance heterostructured organic light-emitting field effect transistors. *ACS Appl. Mater. Interfaces* **2017**, *9*, 2711−2719.

(32) Törmä, P.; Barnes, W. L. Strong coupling between surface plasmon polaritons and emitters: a review. *Rep. Prog. Phys.* **2015**, *78*, 013901.

(33) Stranius, K.; Hertzog, M.; Börjesson, K. Selective manipulation of electronically excited states through strong lightmatter interactions. *Nat. Commun.* **2018**, *9*, 2273.

(34) Polak, D.; Jayaprakash, R.; Leventis, A.; Fallon, K. J.; Coulthard, H.; Petty, A. J.; Anthony, J.; Bronstein, H.; Lidzey, D. G.; Clark, J.; Musser, A. J. Manipulating matter with strong coupling: harvesting triplet excitons in organic exciton microcavities. 2018, arXiv:1806.09990. arXiv.org e-Print archive. https://arxiv.org/abs/1806.09990.

(35) Penfold, T. J.; Dias, F. B.; Monkman, A. P. The theory of thermally activated delayed fluorescence for organic light emitting diodes. *Chem. Commun.* **2018**, *54*, 3926−3935.

(36) Liu, Y.; Li, C.; Ren, Z.; Yan, S.; Bryce, M. R. All-organic thermally activated delayed fluorescence materials for organic light-emitting diodes. *Nature Reviews Materials* **2018**, *3*, 18020.

(37) Bachevillier, S.; Yuan, H.; Strang, A.; Levitsky, A.; Frey, G. L.; Hafner, A.; Bradley, D. D. C.; Stavrinou, P. N.; Stingelin, N. Fully SolutionProcessed Photonic Structures from Inorganic/Organic Molecular Hybrid Materials and Commodity Polymers. *Adv. Funct. Mater.* **2019**, *29*, 1808152.

(38) Song, H.; Singer, K.; Lott, J.; Wu, Y.; Zhou, J.; Andrews, J.; Baer, E.; Hiltner, A.; Weder, C. Continuous melt processing of all-polymer distributed feedback lasers. *J. Mater. Chem.* **2009**, *19*, 7520.

(39) Chan, C.-Y.; Tanaka, M.; Nakanotani, H.; Adachi, C. Efficient and stable sky-blue delayed fluorescence organic light-emitting diodes with CIEy below 0.4. *Nat. Commun.* **2018**, *9*, 5036.

(40) Lee, J.-H.; Chen, C.-H.; Lee, P.-H.; Lin, H.-Y.; Leung, M.-k.; Chiu, T.-L.; Lin, C.-F. Blue organic light-emitting diodes: current status, challenges, and future outlook. *J. Mater. Chem. C* **2019**, *7*, 5874−5888.

(41) Daskalakis, K. S.; Väkeväinen, A. I.; Martikainen, J.-P.; Hakala, T. K.; Törmä, P. Ultrafast Pulse Generation in an Organic Nanoparticle-Array Laser. *Nano Lett.* **2018**, *18*, 2658−2665.